

## **Spatial distribution of microseisms at Turtle Mountain**

Zuolin Chen, Robert Stewart, Henry Bland and Jeff Thurston

### **ABSTRACT**

Comparison between the distributions of the microseismic events and topography, tectonic weaknesses and the historic mine works suggests that movement along thrust faults and induced fractures within the hanging walls of thrust faults may be the source of ongoing microseismicity in the region. Generally, these events are related to steep topography above surface exposures of thrust faults on the mountain's flanks. Further anecdotal evidence for this is the observation of rockslides on only the steep eastern flank. No microseismic hypocentre locations are on, or below, the gentle lower portions of northern and southern flanks. Further, swarms of events have been observed. These tend to originate from sources 1-1.5 km deep beneath the surface of the Frank Slide debris. A relatively few microseismic events correspond to the remaining mine works.

### **INTRODUCTION**

Early and recent geological studies (Allan, 1933; Jones, 1993) attribute the 1903 Frank Slide to either pre-existing fractures or the Frank coal mine works. Microseisms provide direct evidence for the movement of fractures, or fracture zones, as well as for localized tectonic activity and thus may help distinguish causes of the rock slides. Microseismic monitoring in the Turtle Mountain area was first carried out from June to September of 1981 by Earth Sciences Division of Alberta Environment using a single monitoring station (Weichert and Horner, 1981). During this time, three local swarms of microseisms were recorded. Because only a single station was deployed, locating the origins of these events is not possible. However, it was possible to conclude from this initial monitoring effort that the events were localized and of small magnitude. This in turn led to a more comprehensive effort to evaluate the local seismicity. Alberta Environment established a six-station monitoring array on the eastern flank of Turtle Mountain and recorded data from November of 1986 until June 1996 (Bingham, 1996).

In this paper, we discuss our recent efforts to locate events using the seismograms from the six-station array. Also, corresponding lateral and vertical errors of earthquake locations are evaluated. By comparing the distribution of the seismic events with topography, local fault zones and the trend of the mine tunnel, we conclude that tectonic activity within Turtle Mountain likely contributed to the Frank Slide.

### **SEISMIC ARRAY AND DATA PROCESSING**

#### **SEISMIC ARRAY**

The seismic array, comprising six one-channel stations deployed for monitoring the local seismicity within and around Turtle Mountain, is discussed in detail by Bingham (1986). Briefly, this monitoring array consists of two smaller three-station arrays called the FARM and FRANK sub-arrays. The FARM sub-array was deployed 1.5 km southeast of the Turtle Mountain summit, and included stations denoted TMA, TMB and TMC. The FRANK sub-array was located on the rugged east slopes of Turtle Mountain, and

comprised stations denoted TMD, TME and TMF. Details of the positions of the six stations are shown in Table 1.

Table 1. Seismic array and station locations. Locations are given in the 3 degree Transverse Mercator coordinate system, where 114° W and the Equator are regarded as the origins of W-E(x) and N-S (y) directions, and elevation above sea level is regarded as the z direction. For convenience, the origin of the coordinate system is shifted to x=-30870 m, and y = 5491500 m horizontally; zero depth reference level is selected at 2200 m of elevation, which is approximately the height of the Turtle Mountain summit.

Sub-array	Station code	x (m)	y (m)	Shifted x (m)	Shifted y (m)	Depth (m)
FRANK	TMD	-28869.091	5493562.67	2000.91	2062.67	659.0
	TME	-29433.437	5493048.30	1436.56	1548.30	182.0
	TMF	-28842.527	5492973.93	2027.47	1473.93	557.0
FARM	TMA	-28303.577	5491878.16	2566.42	378.16	819.0
	TMB	-28285.538	5492096.06	2584.46	596.06	801.0
	TMC	-28156.685	5491948.70	2716.32	448.70	818.0

All six stations used a single short period (1 s) Teledyne Geotech S-500 seismometer, and all were synchronized in time.

#### TIMING OF P AND S EVENTS

The precision of first break times of P waves from the digital seismograms is of the order of sampling interval (0.005 second). This precision may be degraded somewhat, depending largely on the sharpness of the signal. Generally, the 90% error extent of the first break time of the P phase is considered to be  $\pm 0.005$  seconds.

As the first break of S phases is often overprinted by the P-coda waves, for many events it may be difficult to determine the onset of the shear event precisely, especially in the case of local events, where P coda waves are strong and have undergone little attenuation. In these cases the S-phase pick is mainly based on the distinguishing characteristics of the lower frequencies, higher amplitudes in the P coda, and an abrupt phase change (Figure 1).

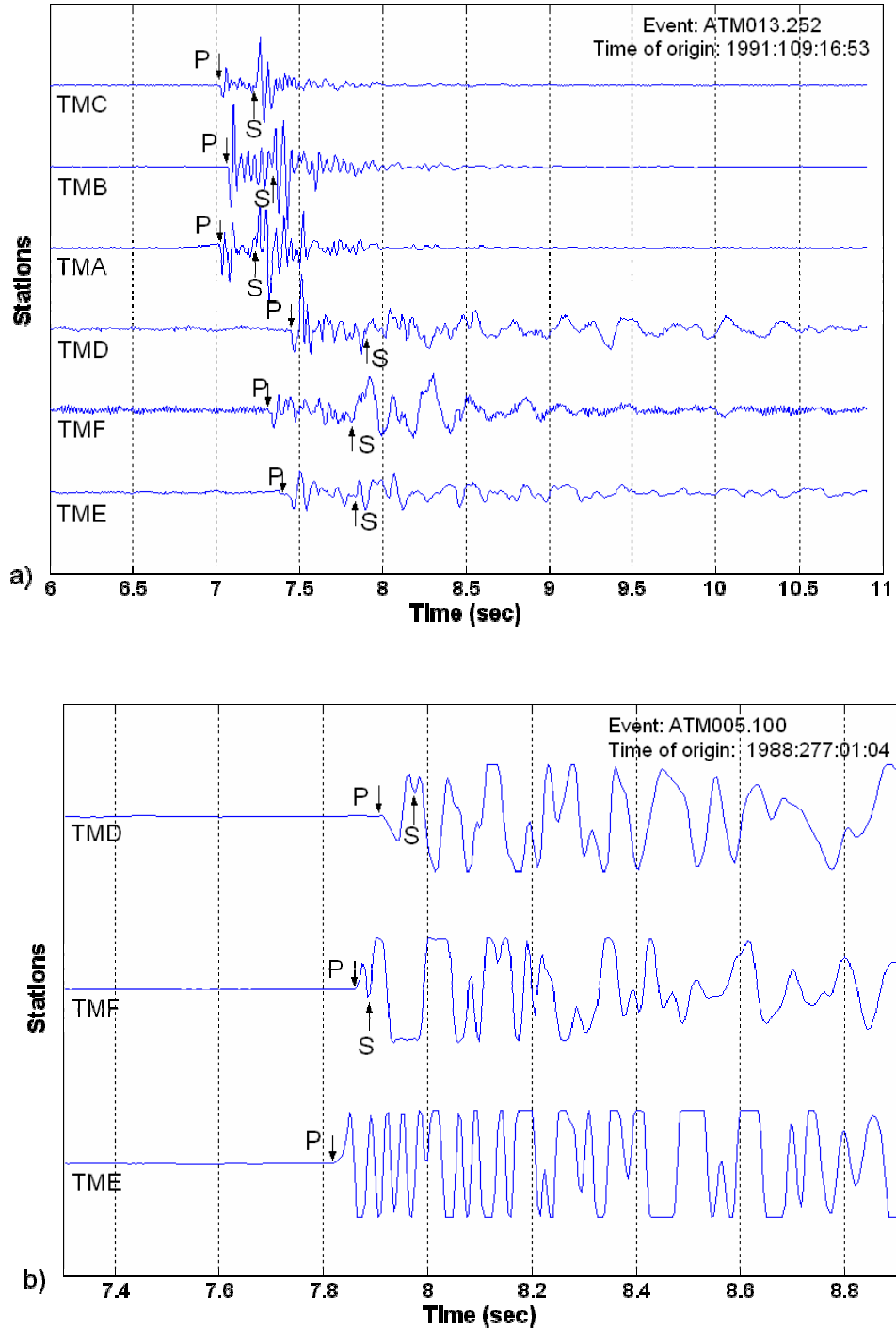


FIG. 1. a) Seismogram of a microseism recorded in April, 1991 by the FRANK and FARM sub-arrays. Stations codes are shown at the beginning of each record. The arrival times of P, S phases are indicated by arrows. The gain of FRANK sub-array is enlarged to make it easier to distinguish amplitudes of P and S phases. b) Seismogram of a microseism recorded in October 1988 by the FRANK sub-array. Annotation is as in Figure 1a. The S phase at TME is not picked due to the short S-P time interval and the mixture of waveforms. This event likely occurred very close to TME station.

In our experience with the data from Turtle Mountain, phase changes are the most common means for identifying the arrival of the S phase for a local event. Nearly contemporaneous phase changes on multiple seismograms provide evidence that a phase change is due to an S event. Figure 1b shows an example in which a local event close to TME with nearly coincidental, and abrupt, phase changes in the adjacent stations (TMD and TMF). Because of the difficulty in identifying S events, the 90% error extent of S phase is regarded to be  $\pm 0.050$  s.

## VELOCITY MODEL AND HYPOCENTER LOCATION

We used a homogeneous model with a P velocity of 4.7 km/s to locate hypocenters using the program HYPOMH (Hirata and Matsu'ura, 1987). This algorithm finds the optimum location which minimizes the observed and predicted travel time residuals of P and S phases of an event, and calculates the corresponding one-standard-deviation lateral and vertical errors. The zero reference level is set at 2200 m of elevation in the velocity model as well. The initial point for searching the locations of the events is assigned at TME, and the search radii are 6.6 km laterally, and 5 km vertically.

## RESULTS

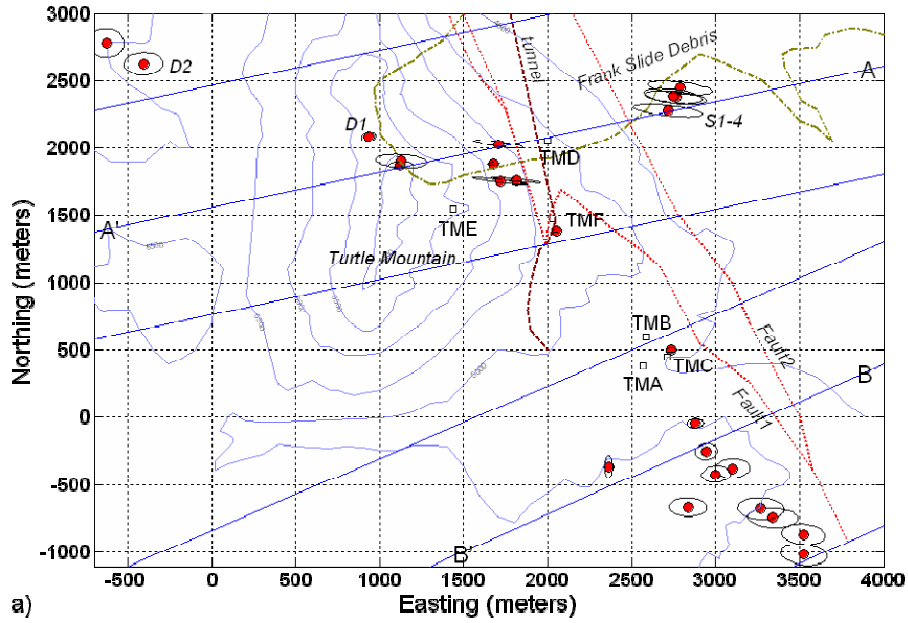
### Events recorded and located by two sub-arrays

Twenty-five microseisms are clearly recorded by both sub-arrays. The event codes, times of origin, locations of hypocentres and numbers of P and S phases used in the hypocenter locating processes are listed in Table 2. Figure 2 shows the hypocentre locations and their reliabilities (lateral and vertical one-standard-deviation error ellipses). Local topography, the extent of debris of Frank Slide, major tectonic fracture zones and the mine tunnel are also shown. Note Fault 1 and Fault 2 are splays of the Turtle Mountain Thrust (Map1829A, 1993). Projecting the trace of Fault 1 onto a horizontal plane makes it clear that the strike of this fault changes between TMB and TMF. The general strikes of northern and southern parts of Fault 1 are approximately NW 16° and NW 29° respectively. The general strike of Fault 2 is approximately NW 23° (similar to the strike of the southern part of Fault 1). Profiles A-A' and B-B' (Figure 2c and 2d) are respectively perpendicular to the strike of the northern and southern segments of Fault 1. Lines A-A' and B-B' represent the directions of two profiles perpendicular to the general strikes of the different pieces of Fault 1.

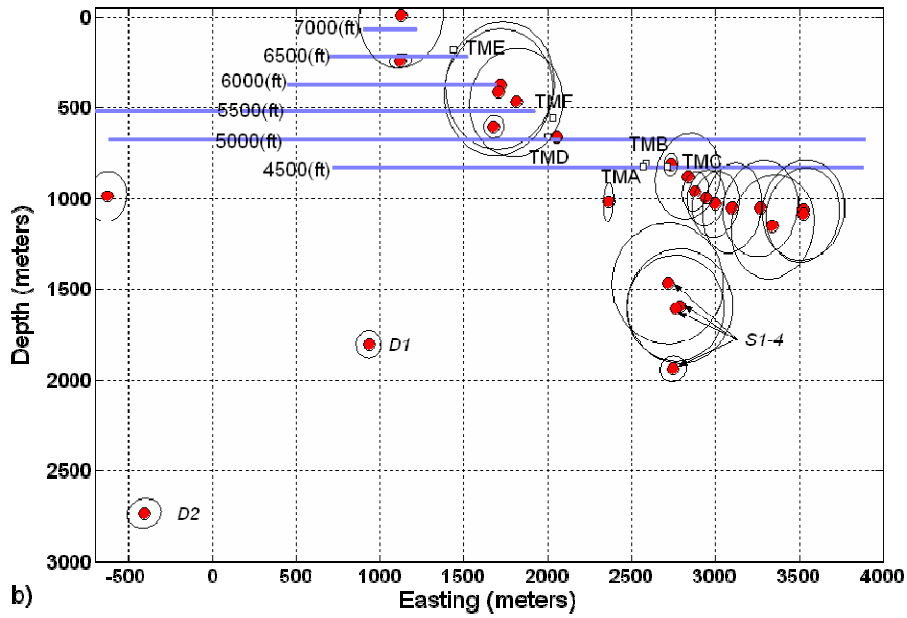
Seven of the twenty-five events are at or near (shallower than 200 m) the surface beneath the south peak and eastern slopes of Turtle Mountain. Projecting onto profile A-A' the distribution of these events together with Fault 1, and the mine tunnel highlights the spatial relationship between them (Figure 2c). One surface event (ATM014.210) coincides with the mine tunnel. The small error extent of this event makes it likely that this microseism occurred in or near the mine tunnel.

Two well resolved (lateral and vertical one-standard-deviation errors of only about 100 m) deeper events occurred beneath the west side of Turtle Mountain. *D1* is approximately 1800 m and *D2* is deeper than 2700 m. Assuming Fault 1 and 2 dip at 40-50° (Map1829A, 1993) in the subsurface, the *D1* is either close to the plane of Fault 1 or

within the hanging wall of Fault 2. Likewise, the hypocentre of *D2* is close to the plane of Fault 1.



a)



b)

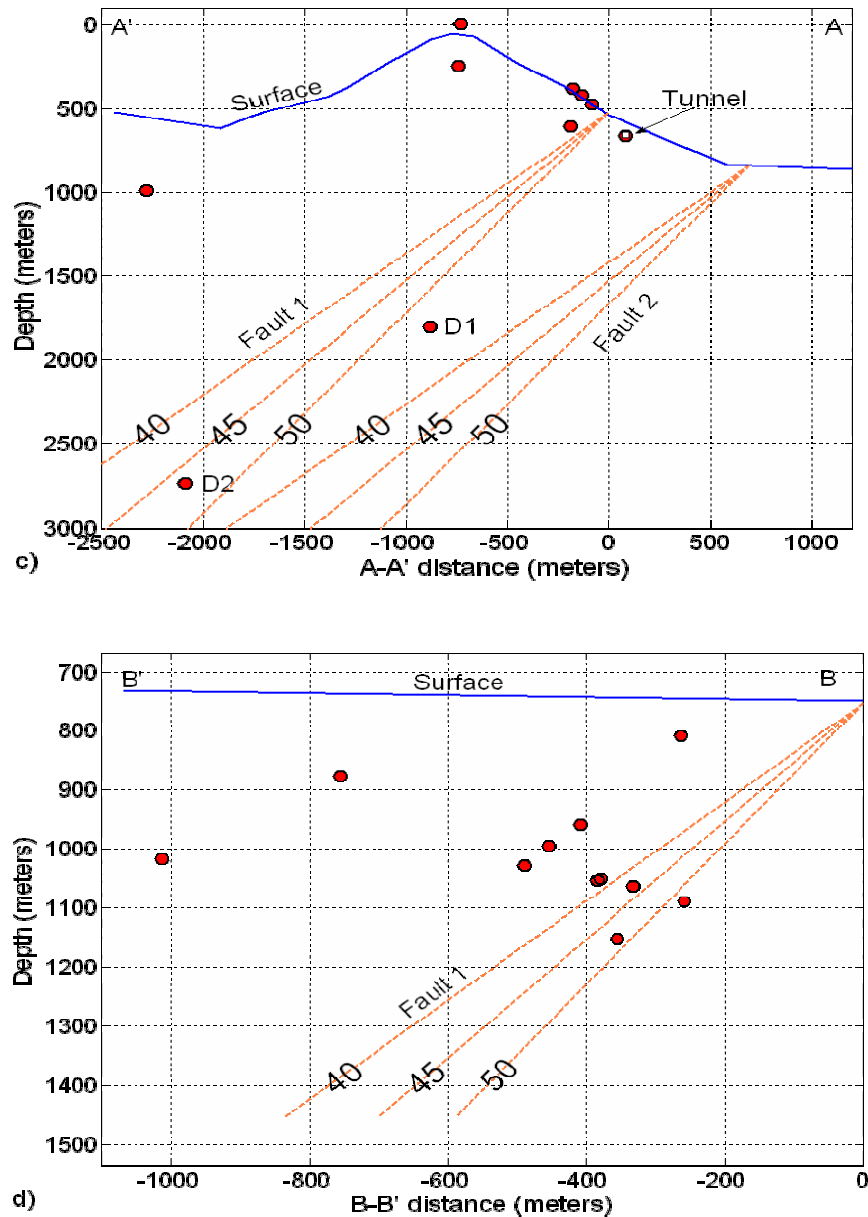


FIG. 2. a) Lateral distribution of hypocenters (dots) and corresponding one-standard-deviation error ellipses of earthquakes located by both sub-arrays. Stations are marked by open squares. Map shows the major contours of Turtle Mountain and the adjacent study areas. Two thrust faults are marked by dotted lines; mine tunnel is indicated by a dashed line. The boundary of Frank Slide debris is indicated by a dash-dotted line. *D1*, *D2* is two deeper events; *S1-4* is four events occurred below southeastern boundary of Frank Slide. b) Easting-depth cross section of vertical hypocenter distribution and one-standard-deviation error ellipses. Elevations of contours are shown in feet. Faults with possible dip angles (40°, 45°, and 50°) are plotted in dashed lines. Horizontal axis represents the lateral distance from the surface exposure of Fault 1. c) Hypocenters projected onto A-A'. The width of the profile is marked by the two adjacent solid parallel lines. The topography of is based on the topography along A-A'. Faults with possible dip angles (40°, 45°, and 50°) are plotted with dashed lines. d) Hypocenters projected onto B-B'. The width of the profile is marked by the two adjacent solid parallel lines. The topography of profile is based on the topography along B-B'. The horizontal axis represents the lateral distance from the surface exposure of Fault 1.

Eleven of the events are distributed southwest of, and roughly parallel to, the southern part of Fault 1 (Figure 2a) mostly between 300 and 400 m below the surface. Overlaying these events on the subsurface projection of Fault 1, (Figure 2d) suggests that these events are either along the plane, or are within the hanging wall of Fault 1.

Four events (*SI-4*) shown on Figure 2, exhibit similar waveforms and occurred within a short time period (about 44 minutes). These are located in a depth range of 1450-1950 m below the southeastern boundary of the Frank Slide debris. Their similar characteristics and proximity suggest these are a cluster of earthquakes. Clustering of earthquakes is discussed in more detail in the following section.

Table 2. Summary of hypocenters of the microseisms located by both sub-arrays. Event codes, times of origin, locations of hypocenters and numbers of P, S phases used in the hypocenter locating processes are listed.

Eq. #	Event Code	Time of origin					Location of hypocenter			Number of phases used	
		yy	dd	hh	mm	ss	x (m)	y (m)	z (m)	P	S
1	ATM003.337	1987	257	17	11	47	2746.9	2387.3	1938.8	5	3
2	ATM003.338	1987	257	17	29	05	2787.7	2446.4	1592.9	5	5
3	ATM003.339	1987	257	17	33	54	2762.3	2376.2	1604.3	5	4
4	ATM003.340	1987	257	17	55	02	2716.4	2281.4	1468.4	5	4
5	ATM013.088	1991	044	14	41	48	1120.1	1876.8	240.7	6	6
6	ATM013.090	1991	044	23	00	43	3535.2	-888.2	1099.4	6	6
7	ATM013.091	1991	045	06	25	54	2734.2	497.0	806.7	6	4
8	ATM013.113	1991	052	22	31	49	-405.5	2626.8	2730.5	6	2
9	ATM013.175	1991	075	17	35	01	3463.8	-907.3	1052.7	6	6
10	ATM013.215	1991	096	08	39	30	1696.3	2049.9	414.8	6	6
11	ATM013.216A	1991	096	09	14	48	1677.5	1884.8	604.2	6	4
12	ATM013.216B	1991	096	09	14	49	1808.9	1771.3	472.6	6	4
13	ATM013.224	1991	101	09	39	10	2950.5	-253.1	980.3	6	6
14	ATM013.233	1991	102	23	22	26	3017.2	-444.6	1026.7	6	6
15	ATM013.235	1991	103	07	33	11	2834.1	-663.5	879.7	6	6
16	ATM013.237	1991	103	09	15	15	1709.4	1759.9	378.4	6	4
17	ATM013.238	1991	103	15	08	27	1128.9	1900.2	-0.59	6	2
18	ATM013.252	1991	109	16	53	51	3358.9	-763.6	1148.2	6	6
19	ATM013.278	1991	118	09	02	04	2888.7	-43.4	929.3	6	6
20	ATM013.330	1991	138	13	21	24	3261.6	-654.5	1054.1	6	4
21	ATM013.333	1991	138	19	53	40	-629.6	2777.8	994.3	6	5
22	ATM013.340	1991	142	21	04	27	2363.1	-361.4	1021.1	6	3
23	ATM013.357	1991	150	20	33	42	933.8	2089.6	1803.9	6	4
24	ATM014.150	1991	223	17	58	03	3051.4	-490.4	1056.1	5	5
25	ATM014.210	1991	259	20	46	36	2053.0	1385.2	659.0	6	4

## EARTHQUAKE SWARMS

Four earthquake swarms have been detected in the vicinity of Turtle Mountain (Table 3). These appear as event clusters with nearly identical waveforms (Figure 3). Weichert and Horner (1981) reported three localized swarms of microseisms occurring from June to September, 1981.

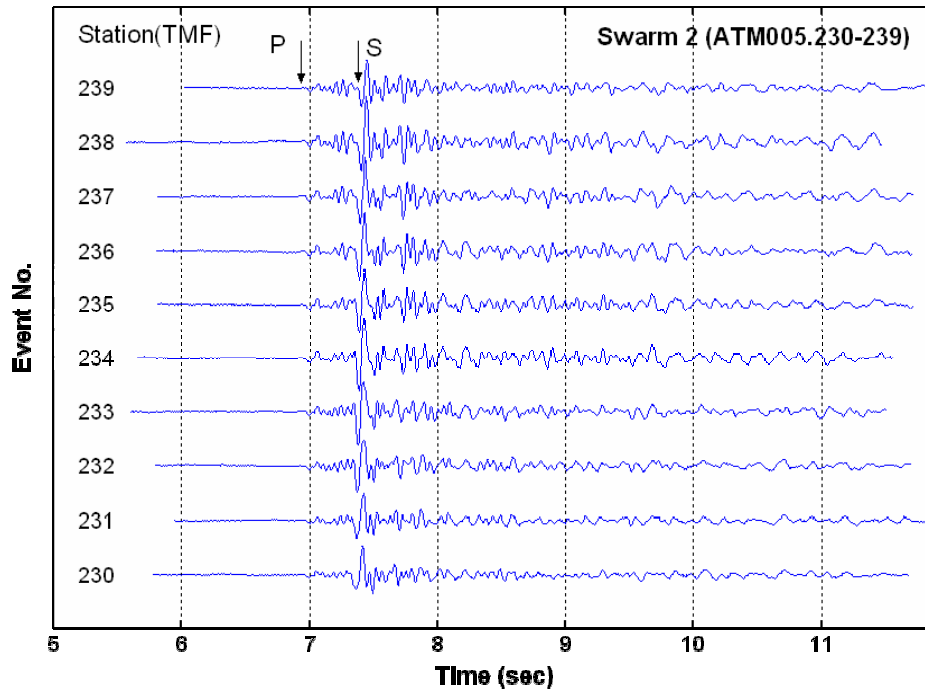


FIG. 3. Seismograms of ten microseisms of Swarm 2 recorded at TMF. Plotting ranges of seismograms are adjusted to make the positions of P, S phases easier to compare from trace to trace.

Of the four earthquake swarms observed by the six-station array, three feature relatively distinct first arrival times of P and S phases and thus are usable for hypocentre location.

The first three swarms occurred at the end of 1988, and Swarm 4 occurred at the beginning of 1989. The duration times of Swarms 1 and 2 are 87 and 43 minutes; Swarm 3 occurred in two stages with a pause of about 10 hours; Swarm 4 also can be divided into two long stages with a pause of nearly 3 days. Note swarms with time durations of a few hours have been reported elsewhere (Frémont and Malone, 1987). The number of events of each microseism swarm ranges from 10 to 20.

Locations of hypocenters from Swarms 1-3 are shown in Figure 4-6. The relatively large station spacing of the stations of the FRANK sub-array, results in locations with large errors, particularly for events that occurred farthest from the sub-array.

All the hypocenters of Swarm 1 are located in two groups. Events from both groups originate between 1.7 and 2.3 km from the reference depth (i.e. the Turtle Mountain summit) approximately 1 km below surface. The hypocentre locations from one of the groups have relatively small errors. This group of events emanate from below the southern boundary of Frank Slide debris. The hypocentre locations of the other group are less accurate, although these events seem to be distributed below the eastern boundary of the slide debris.

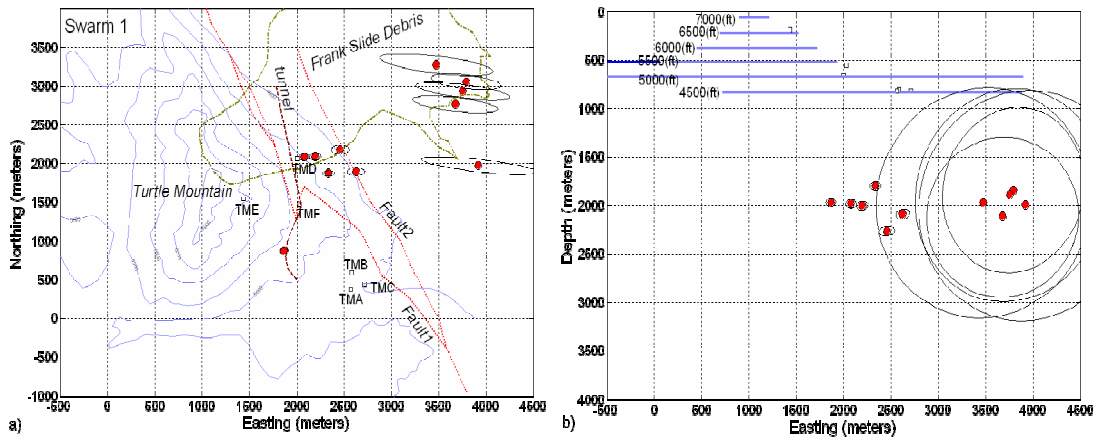


FIG. 4. a) Lateral distribution of hypocenters (dots) and the corresponding one-standard-deviation error ellipses of earthquakes in Swarm 1 located by the FRANK sub-array. Annotation is as in Figure 2a. b) Easting-depth cross section of vertical hypocenter distribution and one-standard-deviation error ellipses. Elevations of contours are shown in feet.

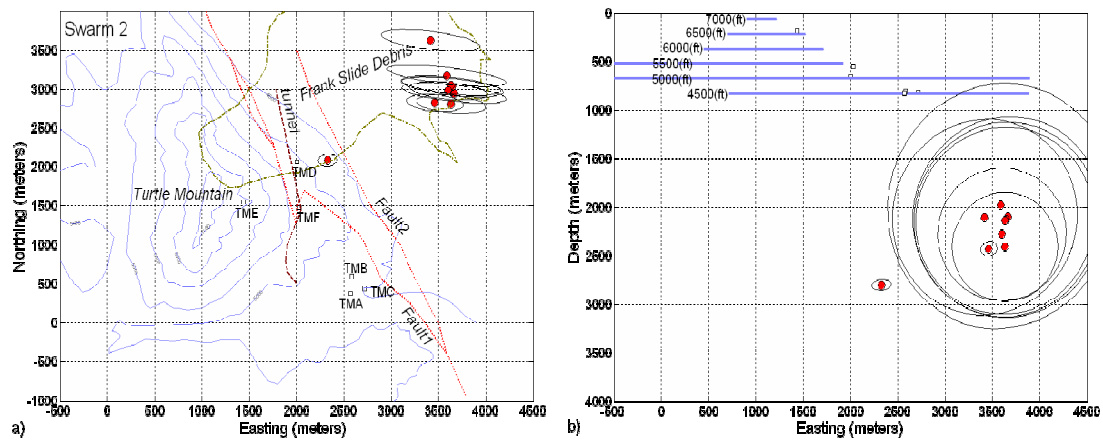


FIG. 5. a) Lateral distribution of hypocenters (dots) and the corresponding one-standard-deviation error ellipses of earthquakes in Swarm 2 located by the FRANK sub-array. Annotation is as in Figure 2a. b) Easting-depth cross section of vertical hypocenter distribution and one-standard-deviation error ellipses. Elevations of contours are shown in feet.

Amongst the three locatable swarms, the waveforms of events from Swarm 2 are most similar. All but one of the hypocenter locations of this Swarm 2 concentrated in a small lateral space of 300x500m (Figure 5a). Like the second group of Swarm 1, Swarm 2 occurred beneath the eastern boundary of the Frank Slide debris. Further, most

hypocentre depths are between 1 and 1.5 km below the surface (Figure 5b). The error extent of the swarm is large due to its position relative to the FRANK sub-array.

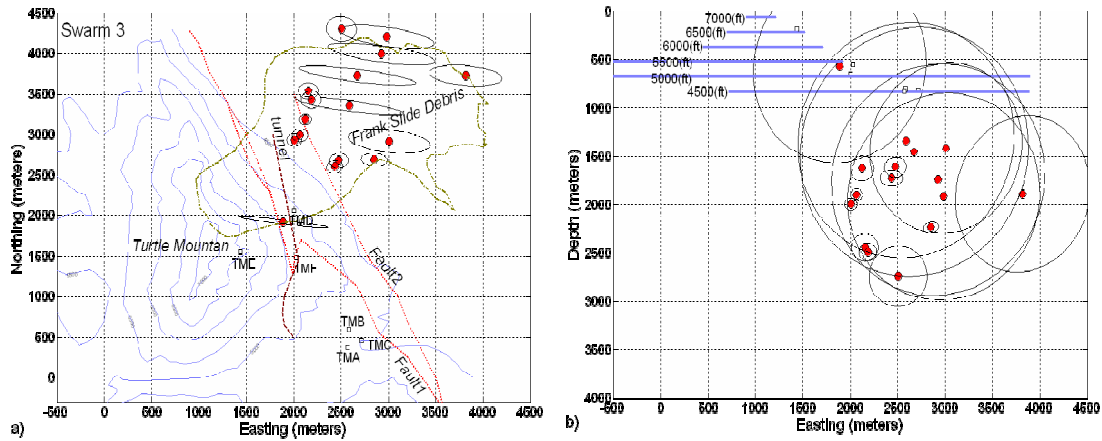


FIG. 6. a) Lateral distribution of hypocenters (dots) and corresponding one-standard-deviation error ellipses of earthquakes in Swarm 3 located by the FRANK sub-array. Annotation is as in Figure 2a. b) Easting-depth cross section of vertical hypocenter distribution and one-standard-deviation error ellipses. Elevations of contours are shown in feet.

Table 3. Event code, start time, ending time, duration times and event numbers of the four swarms detected by FRANK sub-arrays during the observation period. Swarm 3 and 4 are divided into two stages with pause times of ten hours and three days.

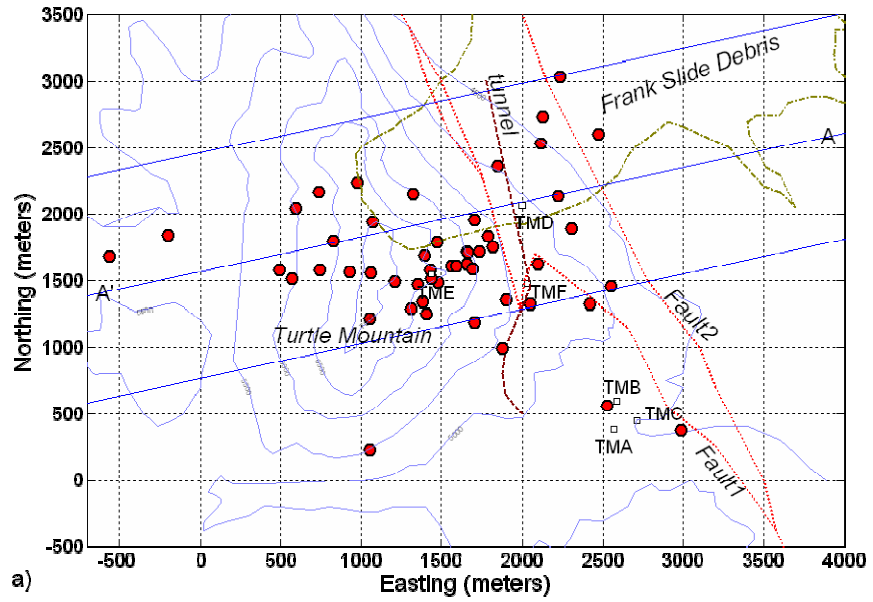
Swarm #	Event Code	Start time				Ending time				Duration time (m)	Total events
		yy	dd	hh	mm	yy	dd	hh	mm		
Swarm 1	ATM005.215-224	1988	323	21	51	1988	323	23	18	87	10
Swarm 2	ATM005.230-239	1988	325	12	18	1988	325	13	01	43	10
Swarm 3	ATM005.247-255	1988	327	04	15	1988	327	05	51	96	16
	ATM005.259-265	1988	328	16	27	1988	328	17	11	44	
Swarm 4	ATM006.136-153 (no138,140,148)	1989	035	02	06	1989	035	09	45	459	19
	ATM006.168-171	1989	038	05	09	1989	038	10	01	292	

The nineteen events of Swarm 3 are located below the northeastern half of the Frank Slide debris just northwest of Swarms 1 and 2 (Figure 6a). As the previous two swarms, the depth error extent indicates the possible depth range of swarm 3 to be approximately 1 -1.5 km beneath the surface (Figure 6b).

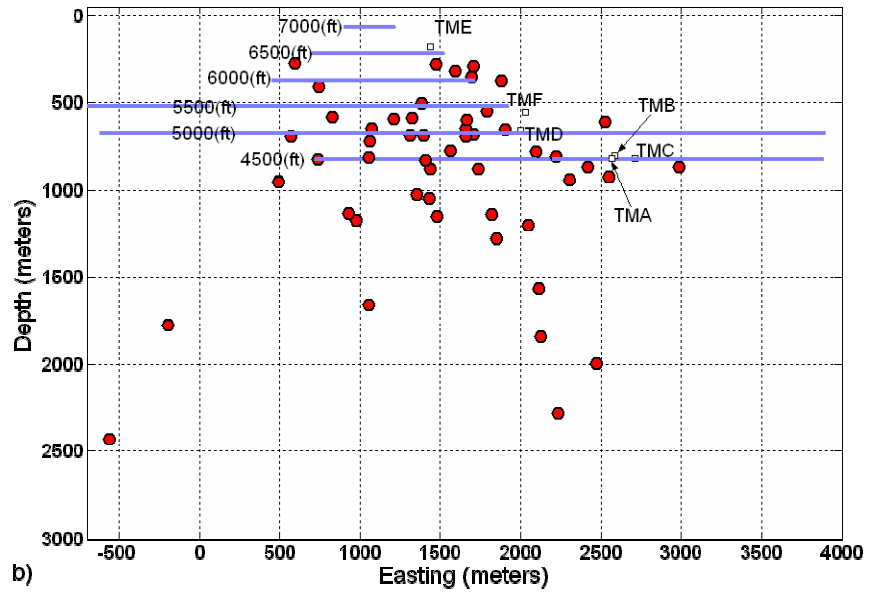
Generally speaking, the centers of microseism swarms occurred about 1-2 km northeast of the FRANK array or 3-4 km northeast of the peak of Turtle Mountain. In depth, they are approximately 1-1.5 km beneath the southeastern part of Frank Slide debris.

#### **LOCAL EVENTS LOCATED BY THE FRANK SUB-ARRAY**

Several hundred local microseisms were detected by only the FRANK sub-array. Due to the small epicentral distances between these microseisms and the observation stations, it is occasionally difficult to accurately pick the arrival times of S phases of these events. Of the 53 microseisms detected between November 1986 and the end of 1988 (Figure 7), 38 events are located with an error ellipse of less than 150 meters (Figure 8).



a)



b)

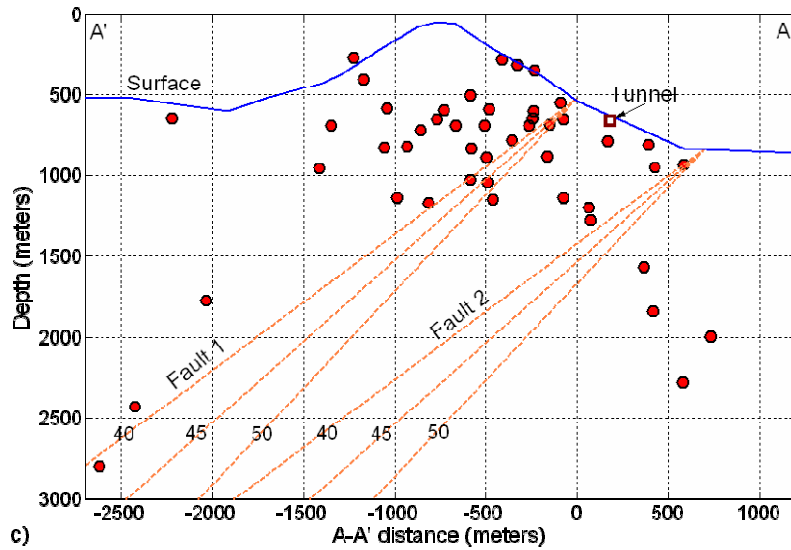
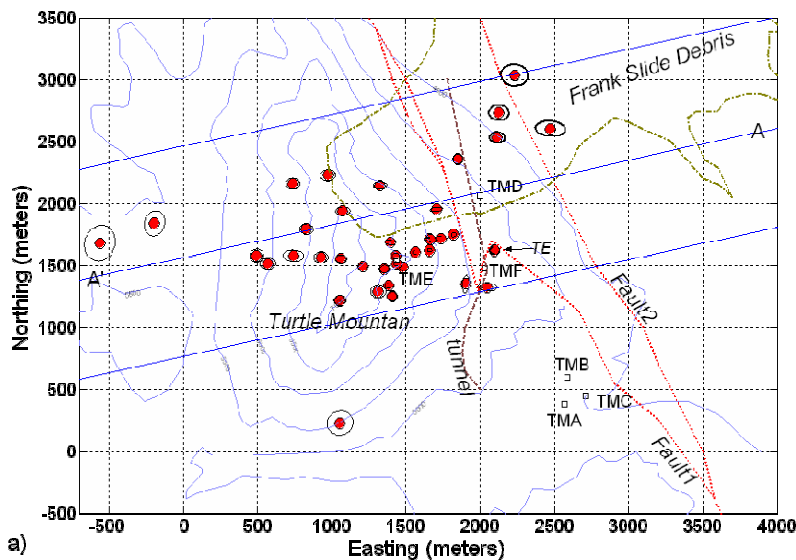


FIG. 7a) Lateral distribution of local microseisms (circles) located by the FRANK sub-array. Annotation is as in Figure 2a. b) Easting-depth cross section of vertical hypocenter distribution. Elevations of contours are shown in feet. c) Hypocenters projected onto A-A'. The width of the profile is marked by the two adjacent solid parallel lines on Figure 7a. The topography is based on the topography along A-A' line. Faults with possible dip angles (40°, 45°, and 50°) are plotted with dashed lines.

From Figure 8, it can be seen that microseisms occurred from the surface to nearly 2.5 km in depth. This depth range is similar to the range of depths of hypocentres located by both the FRANK and FARM sub-arrays. Microseisms are most common beneath the areas adjacent to TME, with depths ranging from 300 meters to more than 1 km. Beneath the peak and western slopes of Turtle Mountain, microseisms seem to occur several hundred meters below the surface. It is interesting that few microseisms are observed on the gentler lower portions of the northern and southern slopes of Turtle Mountain.



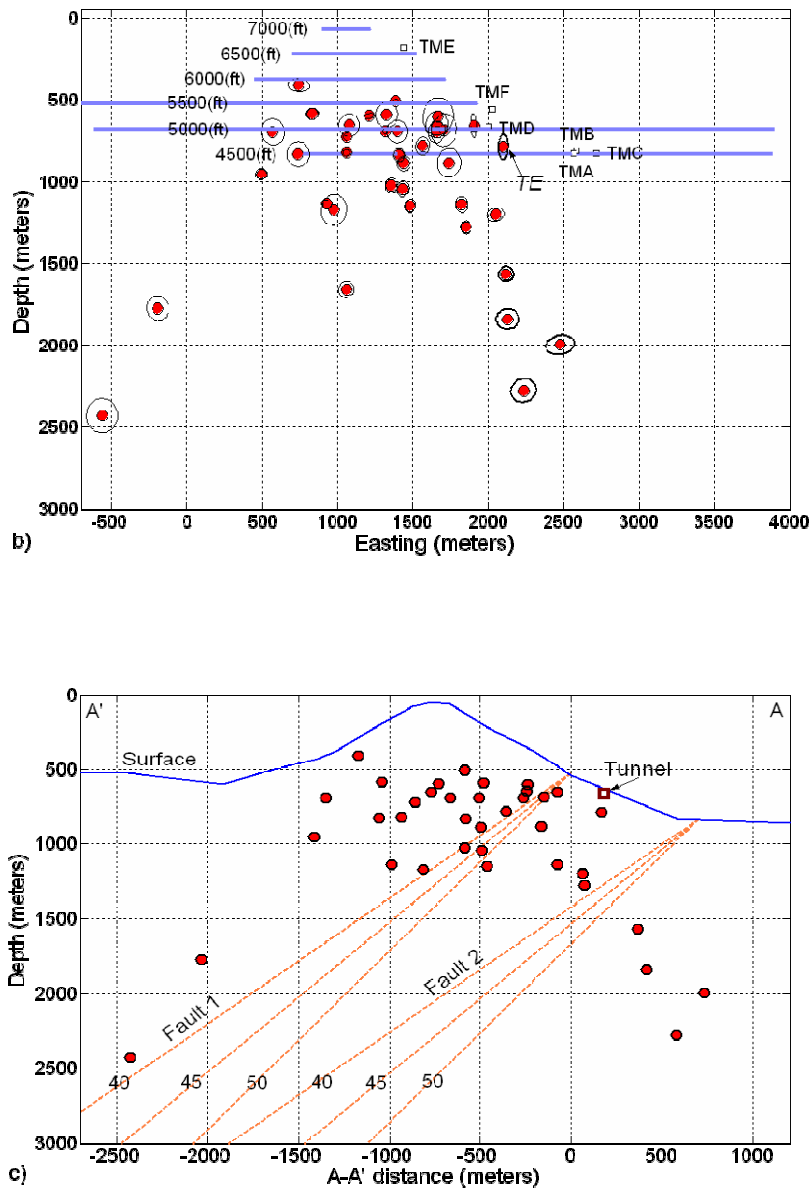


FIG. 8. a) Lateral distribution of hypocenters (dots) and corresponding one-standard-deviation error ellipses of relatively well-resolved earthquakes located by the FRANK sub-array. All three error ellipses have radii less than 150 m. Ellipses of the four deeper events are shown in bold. The event that is apparently along the mine tunnel is named *TE*. Annotation is as in Figure 2a. b) Easting-depth cross section of vertical hypocenter distribution and one-standard-deviation error ellipses. Elevations of contours are shown in feet. c) Hypocenters projected onto A-A'. The width of the profile is marked by the two adjacent solid parallel lines on Figure 8a. The topography is based on the topography along A-A' line. Faults with possible dip angles (40°, 45°, and 50°) are plotted with dashed lines.

Four deeper events (more than 1.5 km in depth) occurred beneath the northeastern slope of the mountain, which coincide with the locations from the three microseism swarms.

The lateral distribution of the hypocenters (Figure 8a) suggests that almost all the events are on the western side of Fault 1, except the four aforementioned deeper events and one shallower event (*TE*) that coincides with the mine tunnel.

From the vertical profile of A-A', it can be seen that microseisms occurred either close to the plane of the thrust Fault 1 or within the hanging wall. Two deeper earthquakes ranging from 1.8-2.4 km in depth also occurred along, or close to the fault.

Few events occurred close to the peak of Turtle Mountain and no events are along the surface of topography in Figure 8b and 8c. However, several events with larger error ellipses are located near the peak and along the surface (Figure 7). Again, this matches the results of the existence of shallow events along the surface derived from the data based on both sub-arrays.

No shallower microseism (less than 1 km in depth) occurred within or beneath the debris of the Frank Slide. The shallower microseisms beneath Turtle Mountain seem to be distributed around the southern rim of the slide path with a width of approximately 500-800 meters.

### DISCUSSION

This study suggests that microseisms in the Turtle Mountain area occur at different depths and for different reasons. From shallow to deep, the origins of the microseisms might be divided into several types: along the topographic surface, along fault planes, within hanging walls, along the mine tunnel, and deep swarms.

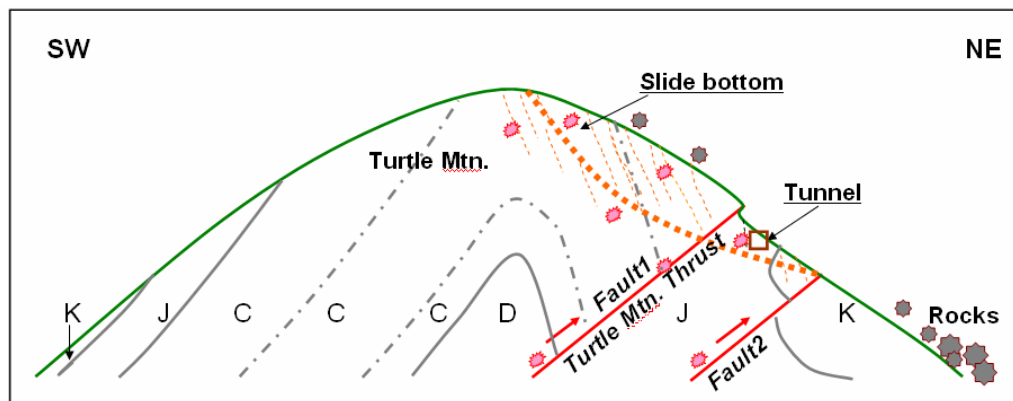


FIG. 9 Schematic SW-NE cross section of Turtle Mountain and the Frank Slide showing the sources of microseisms at Turtle Mountain. The profile crosses the peak of Turtle Mountain and is perpendicular to contour lines on the northeast slope of the mountain. Positions of thrust faults (solid red lines with arrows), mine tunnel (square), bottom of slide body (bold dotted line), fractures (dotted lines) and hypocenters of related possible microseisms are also shown. Boundaries between strata are indicated by solid or dot-dashed lines.

The unexpected lack of microseismicity along the remaining mine tunnel (south of TMD station) is reflected by the following factors: Firstly, though TMD, TMF stations were deployed very close to the remaining mine tunnel, the most intensive microseism active area exists near TME station, which is more than 600 meters west. Secondly, most of the microseisms occurred to the west of mine tunnel and parallel to the strike of Fault1, which is approximately 200 meters west of the tunnel. Thirdly, along the southern part of the tunnel, no event was detected and located.

The collapse of the mine tunnel has been blamed for causing the Frank Slide, on the assumption that was too weak to support of the overlying load. Because the peak of Turtle Mountain is just west of the remaining portions of the mine tunnel, the overlying load is still exists. If the assumption is correct, significant microseismicity should be expected along or near the remaining mine tunnel.

Based on the microseismicity, we believe that it is more reasonable to explain landslide was caused by the activity of underlying thrust faults. Figure 9 shows a schematic cross-section speculating on the sources for the observed distribution of microseismic activity prior to the landslide. As the local Fault 1 and Fault 2 are thrust faults and dip toward west, the hanging walls tend to move eastwards. Due to the movement, it weakened the support to the overlying high loads caused by the steep slopes above Fault 1, and caused lots of fractures within the hanging wall. With the development of fracturing on the eastern slope, when the weight of the fracture-laden rock mass surpassed the limit of support, landslide occurred. At present, faults and fractures within the remaining hanging walls are still active in ways of microseism and rock slides on the eastern slope of the mountain (Bingham, 1996).

Regionally, rock slides are common in the southern Canadian Rockies, especially on eastern mountain flanks (Cruden, 1986). Jones (1993) has mapped an ancient major rock slide (roughly ten times the size of the Frank Slide) below Bluff Mountain immediately north of the Frank Slide. North-south striking thrust faults are prevalent beneath the Rockies, and are commonly exposed on eastern flanks. Based on this newly proposed theory, it is easy to explain their occurrence.

The absence of shallower microseisms between Fault 1 and Fault 2 on the eastern slope of Turtle Mountain may be explained by the relatively flat overlying topography, which results in loading that is not sufficiently high to cause microseisms.

The absence of microseisms on the gentle lower portions of northern and southern slopes of Turtle Mountain can be similarly explained, where the overlying loads is much smaller than those on the steeper eastern slope.

The loose debris of the Flank Slide may explain the absence of shallower microseisms associated with the slide path. This is because the slide debris is unconsolidated and the bottom of the slide path slopes relatively gently. Thus, not enough stress accumulates to cause microseisms.

The four local swarms detected during this observation period together with the three local ones reported by the previous study in 1981 confirms the existence of seismic

swarms in the study areas. The positions and depths of the earthquake swarms indicate that the sources are approximately 1-1.5 km beneath the east and southeast boundaries of the Frank Slide debris. This depth range is further constrained by the location of Events *S1-4*, discussed in this paper. These hypocenters and corresponding error extent are based on the homogeneous velocity model. Arrival time difference between a 3-D and homogeneous velocity models at Turtle Mountain, estimated using a 3-D ray-tracing process (Psencik, 1996), indicates that the time difference is in an order of 0.005 s when the epicentral distance is about 1 km (GENNIX, 2004). As the epicentral distances of the swarms are approximately 1 km, such arrival time uncertainty is taken into consideration in the hypocenter location processes. Thus it is surmised that a 3-D velocity model will affect the locations of the microseisms, and their corresponding error ellipses, slightly.

### **CONCLUSIONS**

Based on the above results and discussion, we derived the following conclusions regarding the seismicity at Turtle Mountain and adjacent areas:

1. The pattern of microseisms can be related to local thrust faults, as microseisms occurred intensively within the hanging walls of thrust faults or along the fault planes.
2. Microseisms related to surface fractures were also observed. These events are mainly distributed along the surface of the eastern slope and peak of Turtle Mountain. The deepest of these is approximately 200 meters below the surface.
3. Two events coincide with the remaining mine tunnel. However, most shallow microseismic activity originates near TME; more than 600 meters west of the mine tunnel.
4. On the gentle lower portions of the northern and southern slopes of Turtle Mountain, microseismic activity is not observed. Further, shallower events (less than 1.0 km below surface) do not occur in the Frank Slide debris.
5. Microseismic swarms occurred frequently below the eastern and southeastern boundaries of the Frank Slide. Their depth is between 1 and 1.5 km below the surface.

### **ACKNOWLEDGEMENTS**

The authors would like to thank Dr. Douglas K. Bingham of Alberta Environment for providing the seismic data. We would like to thank Dr. Naoshi Hirata of ERI of the University of Tokyo, Japan for kindly providing us the computer program HYPOMH. We also thank Dr. Rolf Maier and Kevin Hall of CREWES for their helpful comments on this paper.

## REFERENCES

- Allan, J.A., 1931, Report on Stability of Turtle Mountain, Crowsnest District, Alberta. Dept. of Public Works, Edmonton: Alberta Provincial Archives.
- Bingham, D.K., 1996, Seismic monitoring of Turtle Mountain: Internal report, Alberta Environmental Protection. Government of Alberta.
- Cruden, D.M., 1986, Monitoring the south peak of Turtle Mountain, 1980-1985: RMD Report 86/37, Alberta Environment, Edmonton, 59pp.
- Frémont, M.J., Malone, S.D., 1987, High precision relative locations of earthquakes at Mount St. Helens, Washington: *J. Geophys. Res.*, **92**, 10,223-10,236.
- GENNIX, 2004. System design and numerical experiments: Report to Alberta Municipal Affairs, Chapter 2.
- Jones, P.B., 1993, Structural geology of the modern Frank slide and ancient Bluff Mountain Slide, Crowsnest, Alberta: *Bull. Can. Petro. Geol.*, **41**, 232-243.
- Map 1829A, 1993, Geology and structure cross-sections, Blairmore (West Half), Alberta, Scale 1:50000. Geological Survey of Canada.
- Hirata, N., and Matsu'ura, M., 1987, Maximum-likelihood estimation of hypocenter with origin time eliminated using nonlinear inversion technique: *Phys. Earth Planet. Inter.*, **47**, 50-61.
- Psencik, I., 1996, ANRAY Documentation, version 4.20: Report of Geophysical Institute, Acad.Sci. of the Czech Rep.
- Weichert, D.H., and Horner, R.B., 1981, Microseismic monitoring in Blairmore, Alberta: Internal Report 81-4, Earth Physics Branch, Energy, Mines and Resources Canada, Ottawa, 27pp.